This article has been accepted for inclusion in a future issue of this journal. Content is final as presented, with the exception of pagination.

On the CET-Map Ill-Posed Inversion Problem: Theory and Application to GaN HEMTs

Nicola Modolo, Carlo De Santi, *Member, IEEE*, Giulio Baratella, Andrea Minetto, Luca Sayadi, Sebastien Sicre, Gerhard Prechtl, Gaudenzio Meneghesso, *Fellow, IEEE*, Enrico Zanoni, *Life Fellow, IEEE*, and Matteo Meneghini

***Abstract*— Ideally, de-trapping transients in semiconductors originate from discrete energy levels, and the emission profile follows a pure exponential decay; however, it has been widely shown that this rarely happens in real devices, for which capture and emission processes have a strongly stretched exponential shape. Conventional methodologies for capture/emission time constants mapping (CET maps) are based on the double derivative (DD) or bivariate Gaussian (BG) approximation, which may lead to inaccuracies in the presence of complex defect distributions. In this article, we introduce a new methodology, based on the double inverse Laplace transform, to extract the accurate capture-emission time (CET) map of these defects. The proposed approach is compared with the conventional approximated solutions, thus giving insight into whether the error introduced by the simplified approaches can be considered negligible or not. First, to ensure full control of the input parameters, the analysis is carried out on custom-generated functions with different stretching parameters. Then, the developed methodology is used to extract, for the first time, the full capture/emission time map from a power GaN high-electron mobility transistor (HEMT) subjected to positive bias instability (PBI) test. The proposed approach is universal and can be adopted by a wide variety of electronic devices in the presence of charge-trapping processes.**

***Index Terms*— Activation energy distribution, p-GaN high-electron mobility transistors (HEMTs), stretched exponential, surface traps, time-constant profile extraction, trap-state mapping.**

Manuscript received 18 February 2023; revised 8 May 2023; accepted 18 May 2023. The review of this article was arranged by Editor G. I. Ng.
(Corresponding author: Carlo De Santi.)

Nicola Modolo was with the Department of Information Engineering, University of Padova, 35131 Padua, Italy. He is now with Infineon Technologies Austria, 9500 Villach, Austria (e-mail: nicola.modolo@infineon.com).

Carlo De Santi, Gaudenzio Meneghesso, and Enrico Zanoni are with the Department of Information Engineering, University of Padova, 35131 Padua, Italy (e-mail: carlo.desanti@unipd.it; gaudenzio.meneghesso@unipd.it; enrico.zanoni@unipd.it).

Giulio Baratella was with the Department of Information Engineering, University of Padova, 35131 Padua, Italy. He is now with the CMST, IMEC, Ghent University, 9052 Ghent, Belgium (e-mail: giulio.baratella@imec.be).

Andrea Minetto, Luca Sayadi, Sebastien Sicre, and Gerhard Prechtl are with Infineon Technologies Austria, 9500 Villach, Austria (e-mail: andrea.minetto@infineon.com; luca.sayadi@infineon.com; sebastien.sicre@infineon.com; gerhard.prechtl@infineon.com).

Matteo Meneghini is with the Department of Information Engineering, University of Padova, 35131 Padua, Italy, and also with the Department of Physics and Astronomy, University of Padova, 35131 Padova, Italy (e-mail: matteo.meneghini@unipd.it).

Color versions of one or more figures in this article are available at https://doi.org/10.1109/TED.2023.3284806.

Digital Object Identifier 10.1109/TED.2023.3284806

I. Introduction

THE ability to understand, predict, and control the impact of native defects, unintentional contaminants, and dopant impurities assumes great importance when developing new technologies based on innovative materials.

The most common defect characterization technique is deep-level transient spectroscopy (DLTS) [1], [2], [3]. Among the many DLTS techniques, capacitance C-DLTS is based on the automatic acquisition and analysis of capacitance transients on diode structures [4].

Unfortunately, for complex structures such as GaN high-electron mobility transistors (HEMTs), it is difficult to obtain meaningful experimental results based on the analysis of junction capacitance, unless specific test structures are used.

For this reason, other parameters such as threshold voltage and ON-resistance are typically analyzed to detect the presence of trapped charge in the devices: a common technique is drain current transient spectroscopy (DCTS), which can explore the capture and emission kinetics of a trap center from the microseconds to the thousands of seconds time scale [5], [6], [7].

Ideally, the trapping phenomena originate from defects with discrete energy levels, and the DCT profile behaves as a pure exponential decay function ($e^{-t/\tau}$). However, it has been shown that this rarely happens in real HEMTs, where more complex defect distributions and/or surface states can play a significant role [8], [9], [10], [11], [12]: transients are strongly stretched ($e^{-(t/\tau)^{\beta}}$) due to the fact that defects are distributed in energy and/or in space.

The extraction of the time-constant distribution profile has been a long-standing problem for the trap analysis of GaN-based HEMTs [13], [14], [15], [16]. Several approximated approaches have been proposed, including a simple derivative or a multiple exponential fit of the DCTs [17]. In a recent work [18], we demonstrated that a correct extraction of the time-constant distribution of relaxation kinetics can be reconducted to a 1-D mathematical inversion problem whose generalized function can be written in the form of a first-kind

This work is licensed under a Creative Commons Attribution-NonCommercial-NoDerivatives 4.0 License.
For more information, see https://creativecommons.org/licenses/by-nc-nd/4.0/

Freehold Integral equation

$$f(t) = \sum_{i=1}^{k} A_i \cdot \exp\left(-\frac{t}{\tau_i}\right) = \int_0^\infty g(\tau) \cdot k(t,\tau) d\tau \quad (1)$$

where the kernel $k(t, \tau)$ is the pure exponential decay function [19], [20], [21]. Hence, an accurate (not approximated) $g(\tau)$ extraction was obtained by solving the inverse Laplace transform, starting from the experimental transients

$$g(\nu) = L^{-1}\{f(t)\}. \quad (2)$$

On top of this, we demonstrated that the trap states properties can be univocally described, starting from the extracted time-constant distributions at different temperatures.

Nevertheless, an even more intriguing problem arises when not only the emission, but also the capture time evolution is considered, to model how a device behaves after a given stress time, and after a given recovery time. Solving this 2-D problem allows to evaluate the device instability, given a certain operating duty cycle and frequency, thus providing relevant information to circuit designers.

Within this framework, the capture-emission time (CET) map has been proposed by Grasser et al. [22], [23], [24] as a powerful method to visualize the time-constant distribution of single and multiple defects to study BTI in power MOSFETs.

Under the assumption that the occupancy state of a trap can be approximated to a step function, the proposed model describes the charge exchange of independent defects in agreement with a bivariate Gaussian (BG) distribution.

This article aims to give further advancement to this methodology by extending our findings on inverse Laplace transform [18] to a 2-D domain. The main advantage of our approach lies in the fact that the occupancy state of a trap is not approximated to a step function. Therefore, the real-time constant distribution can be extracted. The proposed methodology, namely, Double i-Laplace (DiL), is then compared with the conventional double derivative (DD) and the BG map extraction, thus giving insight into whether the error introduced by these two simplified inversions can be considered negligible or not.

Finally, the developed mathematical framework is used, for the first time, to study threshold voltage instability of normally-OFF power HEMTs submitted to electrical stress. Remarkably, by comparing the time-constant distribution with the iso-frequency and iso-duty-cycle loci, the trajectory of the device instability under different operating conditions can be predicted.

II. One-Dimensional Inversion With Different Stretching Parameters

Before diving into the 2-D domain, it is useful to build a quantitative insight into the time-constant distribution extraction in the 1-D domain.

Referring to (1), a generally accepted method to solve this problem is to simplify it by assuming that the capture and emission kinetics of a single process can be approximated to a step function [25]

$$f(t) = \int_0^\infty g(\tau) \cdot H(t-\tau) d\tau = \int_t^\infty g(\tau) d\tau. \quad (3)$$

Therefore, the approximated time-constant distribution $g(\tau)$ of a given transient $f(t)$ can be calculated as the *derivative* of $f(t)$. For noisy and/or truncated experimental data, the time constant profile can be further approximated to a *Gaussian distribution*. Critically, to the best of the authors' knowledge, a proper comparison between these two methods and the real-time constant distribution has never been investigated in detail.

An early attempt has been proposed by Bisi et al. [17], in which, following the approach of Joh and Del Alamo [13], a realistic time-constant distribution was extracted by brute force fitting with 100 pure exponential decays. Alternatively, as we demonstrated in [18], the inversion problem can be approached mathematically, thus drastically decreasing the number of fitting parameters.

To properly compare derivative, Gaussian, and inverse Laplace extraction, the $f(t)$ function is custom generated as a stretched exponential decay centered in $\tau_0 = 1$ s; this ensures full control of the input parameters. Similar considerations can be extended to the experimental data, whether they are threshold voltage shift (ΔV_{TH}) and/or dynamic ON-resistance (R_{ON}).

Fig. 1 shows the result of the comparison at various values of the stretching factor β. The three distributions are shown with different colors and are presented normalized to their maximum value, to allow an easier visualization and understanding of the difference in shape between them. It should be noted that, since $f(t)$ is custom generated, the Gaussian distribution is simply obtained by fitting the derivative distribution (no need for optimization).

A qualitative explanation of the shape of the spectra can be given as follows. The abscissa of the peak value represents the time constant of the main component of the distribution, i.e., of the individual defect of the defect distribution which is present in the highest equivalent concentration. The area below the curve is proportional to the concentration of electrically active defects causing the experimental transient. An interested reader can find more information in [18].

From a quantitative analysis, a difference in the dominant time constant (τ_{pk}), and distribution profile ($g(\tau)$), can be distinguished. To quantify the robustness of the approximated extractions, the error in the dominant time constant has been calculated as

$$\varepsilon_{pk,G/D} = \frac{\tau_{pk,G/D} - \tau_{pk,L}}{\tau_{pk,L}} \quad (4)$$

where $\tau_{pk,L}$ and $\tau_{pk,G/D}$ are obtained from the i-Laplace, and the Gaussian/derivative method, respectively. Furthermore, the absolute error in the distribution profile has been calculated as

$$\varepsilon_{G/D} = \frac{\int_0^\infty \left|g_{G/D}(\tau) - g_L(\tau)\right| d\tau}{\int_0^\infty \left(\left|g_{G/D}(\tau)\right| + \left|g_L(\tau)\right|\right) d\tau} \quad (5)$$

where $g_L(\tau)$ and $g_{G/D}(\tau)$ correspond to the i-Laplace, and the Gaussian/derivative method, respectively. The result of this comparison is shown in Fig. 2(a) and (b). In particular: 1) the

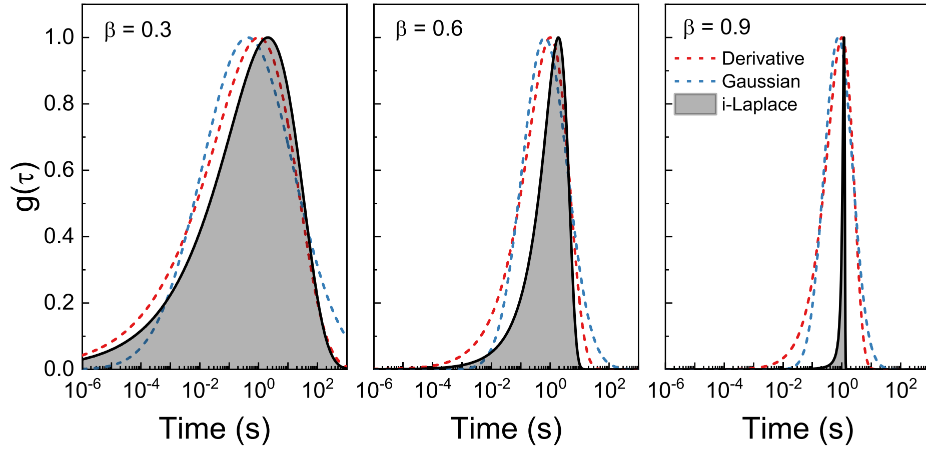

Fig. 1. Time-constant distribution extraction in the 1-D domain from a custom generated stretched exponential decay with varying stretching parameters. Different colors are used to compare the different profiles obtained with different inversion methods, i.e., derivative, Gaussian approximation, and inverse Laplace. The *i*-Laplace method is used as a reference for a realistic τ_i distribution.

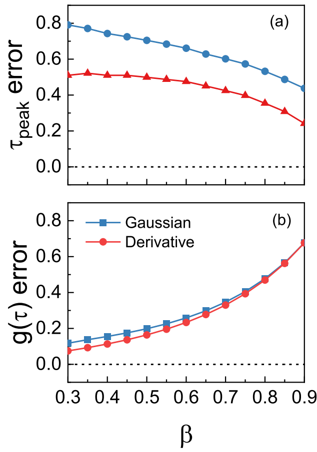

Fig. 2. Error introduced by the derivative and Gaussian extraction to estimate. (a) Dominant time constant. (b) Distribution profile.

higher the β (i.e., the more ideal the exponential), the lower the error to calculate the dominant time constant; and 2) the higher the β, the higher the difference between the distribution profiles.

Also, it can be understood that the assumption that the derivative profile can be approximated to a Gaussian profile is very strong (given the symmetry of the Gaussian distribution). This may lead to overestimating the time-constant distribution for $\tau_i > \tau_0$, and underestimate it for $\tau_i < \tau_0$.

The analysis carried out in this section can be extended to the 2-D case. In the next section the different methodologies, namely, DiL, DD, and BG will be compared for the first time.

In the literature, additional time-constant spectrum extraction methods are reported, based on the Bayesian deconvolution [26]. Since the methods based on Bayesian deconvolution are applied to the derivative of the experimental transient, they share the same issues with the derivative method. As can be noticed in Fig. 2 in [27], the extracted time-constant spectrum is cleaner than the derivative one but still incorrect, since it should be composed only of three Dirac's delta.

III. Two-Dimensional Inversion With Different Stretching Parameters

The basic idea of the CET map is to study the interactions between capture and emission processes by monitoring the recovery kinetics of the device as a function of stress time. Experimentally, the data can be obtained from a matrix of DCT or V_{TH} transient measurements. Physically, assuming a collection of independent defects with a distribution of exponential capture and emission times, the total kinetics can be obtained by summing up the contribution of all defects

$$f(t_c, t_e) = \sum_{i=1}^{m}\sum_{j=1}^{n} A_{ij} \cdot \exp\left(-\frac{t_e}{\tau_i}\right) \cdot \left(1 - \exp\left(-\frac{t_c}{\tau_j}\right)\right). \quad (6)$$

Mathematically, (6) belongs to a class of inverse ill-posed problems, modeled by a first-kind Fredholm integral equation having separable kernels

$$f(t_c, t_e) = \iint_0^\infty g(\tau_c, \tau_e) \cdot k_1(t_c, \tau_c) \cdot k_2(t_e, \tau_e) d\tau_e d\tau_c \quad (7)$$

where $g(\tau_c, \tau_e)$ is the CET distribution ("the map") with dimension (V/s^2), and $k_1(t_c, \tau_c)$, $k_2(t_e, \tau_e)$ are the pure exponential decay functions of the capture and emission process. Within this description, the state of a single defect will be dependent on the specific τ_c/τ_e ratio of the defect, and the device stressing history.

To simplify the integration, Grasser et al. [25] suggested approximating the trap state to the step function, thus giving a very intuitive connection between $f(t_e, t_c)$ and $g(\tau_c, \tau_e)$

$$f(t_c, t_e) = \int_0^{t_c}\int_{t_r}^{\infty} g(\tau_c, \tau_e) d\tau_e d\tau_c. \quad (8)$$

In other words, this means that the DD of $f(t_c, t_e)$ approximates $g(\tau_c, \tau_e)$. Since the experimental window may not be able to capture the device's full kinetics, the additional assumption that the 2-D profile is the tail of a Gaussian distribution is made. Therefore, $g(\tau_c, \tau_e)$ is fit with a BG function.

This article has been accepted for inclusion in a future issue of this journal. Content is final as presented, with the exception of pagination.

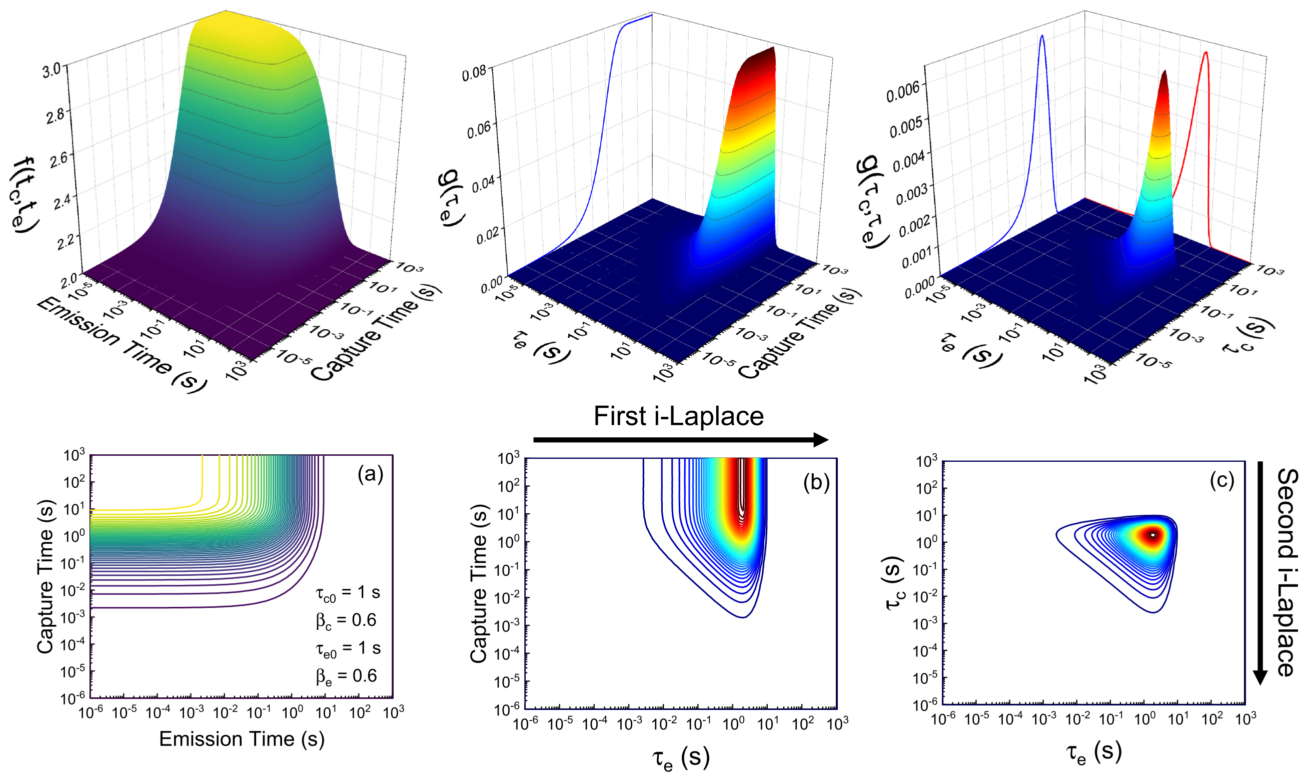

Fig. 3. Time-constant distribution extraction in the 2-D domain. (a) From a custom-generated function, (b) first inversion is performed in the emission, and (c) then capture direction.

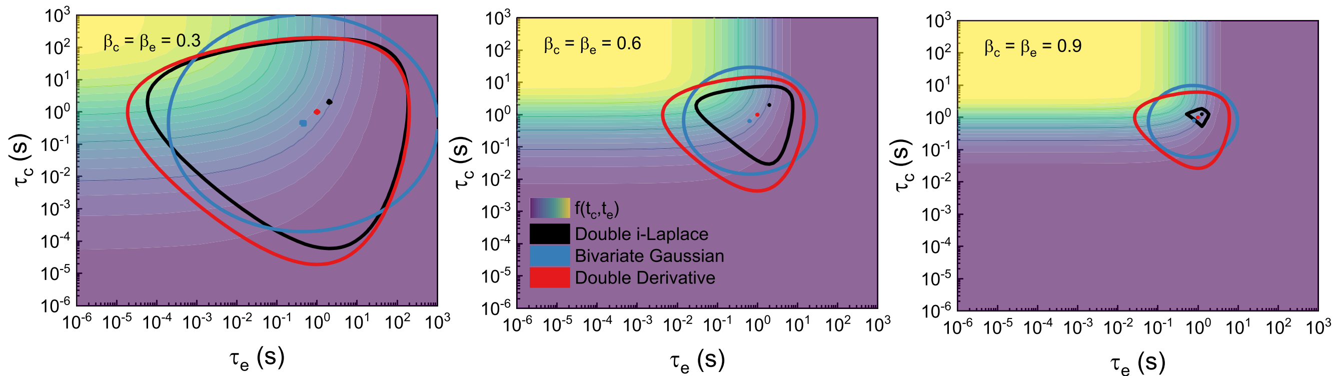

Fig. 4. Contour plot of the extracted time-constant distribution by means of DD (red), BG (blue), and DiL (black) methods at various $\beta_c = \beta_e$. Only the lateral cuts at 10% and 99.9% of the normalized distributions are shown thus highligting the difference in the profile peak and width.

However, as discussed for the 1-D case, these approximations can lead to an over/underestimation of the τ_c/τ_e components. To correctly extract the $g(\tau_c, \tau_e)$ CET map we propose to extend the Euler numerical inversion in [18] to the 2-D domain. Again, to ensure full control of the input parameters, the comparison between the different analytical procedures is carried out on a custom-generated function $f(t_e, t_c)$

$$f(t_c, t_e) = Z_0 + A_0 \cdot \left(1 - \exp\left(-\frac{t_c}{\tau_{c0}}\right)^{\beta_c}\right) \cdot \exp\left(-\frac{t_e}{\tau_{e0}}\right)^{\beta_e} \tag{9}$$

where $Z_0 = 2$, $A_0 = 1$, and for the sake of simplicity, $\tau_{c0} = \tau_{e0} = 1$ s, $\beta_c = \beta_e = 0.6$. The surface and contour plots of the custom matrix are reported in Fig. 3(a). Then, as shown in Fig. 3(b) and (c), the double inversion is performed in the emission first and capture direction. We note here that, contrary to the previously reported DD/Gaussian approximations, Fig. 3(c) shows the real CET map of $f(t_c, t_e)$ without any additional assumption. Note that the peak position in Fig. 3 does not match the set time constant of the stretched exponential function, as discussed in [18].

The comparison between the results obtained with DiL, DD, and BG extraction is shown in Fig. 4 at various $\beta_c = \beta_e$, together with the custom generated $f(t_c, t_e)$. Consistently with the 1-D analysis, a difference in the peak and distribution profile can be distinguished depending on the value of the stretching parameter. The quality of the extraction can be visualized by reconstructing $f(t_c, t_e)$ from the CET map, by

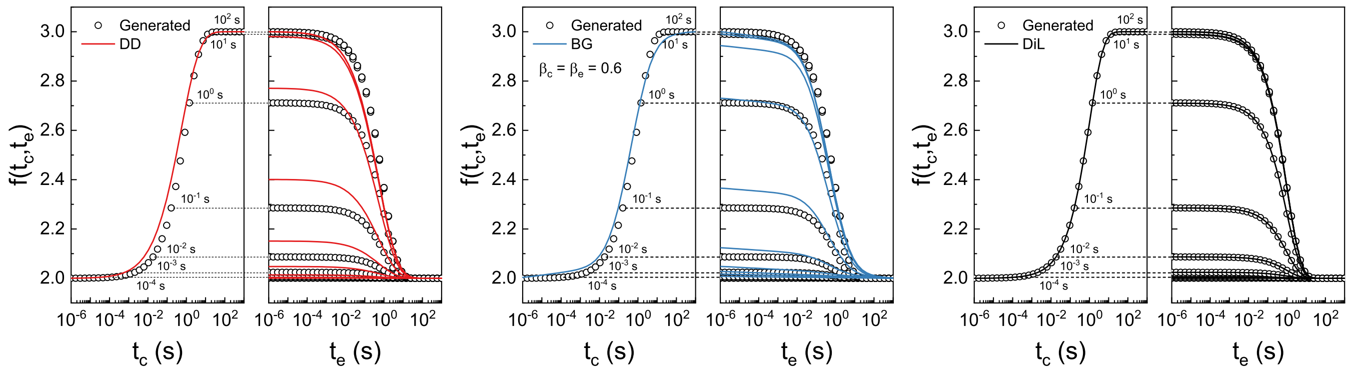

Fig. 5. Comparison between generated $f(t_e, t_c)$ and reconstructed function, where the $g(\tau_c, \tau_e)$ map is obtained by means of (a) DD, (b) BG, and (c) DiL methods. As expected, only the DiL method can correctly reproduce the generated $f(t_e, t_c)$.

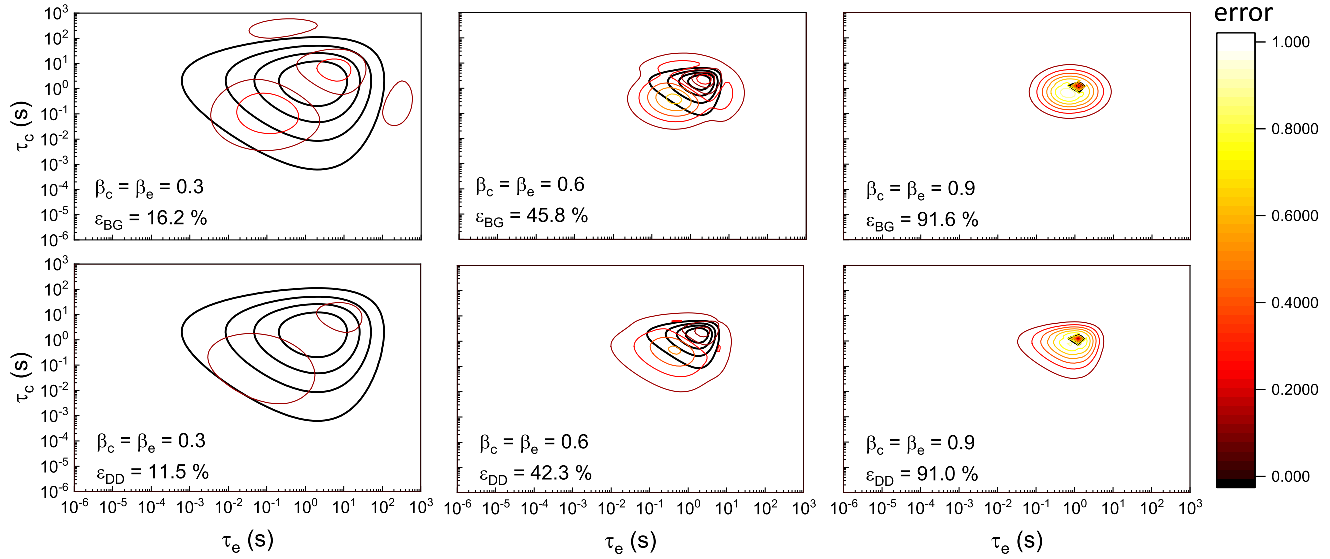

Fig. 6. Contour plot of the point-by-point error introduced by the BG (above) and DD (below) method (from dark red to bright yellow) superimposed to DiL CET map (black) at various $\beta_c = \beta_e$. Consistently with the theory, the lower the β, the smaller the error introduced by the approximation of the occupancy state to a step function.

using (6), where the A_{ij} components correspond to the profiles in Fig. 4. The result of this calculation is shown in Fig. 5, where both the capture and emission kinetics are shown after reconstruction at $\beta_c = \beta_e = 0.6$. The plot shows both the trapping and de-trapping kinetics. While the DiL map perfectly follows $f(t_c, t_e)$, both the DD and BG maps introduce an error. Similar to (5), the absolute error of the $g_{\mathrm{BG/DD}}(\tau_c, \tau_e)$ extraction can be calculated as

$$\varepsilon_{\mathrm{BG/DD}} = \frac{\iint_0^\infty \left|g_{\mathrm{BG/DD}}(\tau_c, \tau_e) - g_{DiL}(\tau_c, \tau_e)\right| d\tau_e d\tau_c}{\iint_0^\infty \left|g_{BG/DD}(\tau_c, \tau_e)\right| + \left|g_{DiL}(\tau_c, \tau_e)\right| d\tau_e d\tau_c}. \tag{10}$$

Fig. 6 shows the contour plot of the point-by-point error introduced by the BG (above) and DD (below) method, in a color coding from dark red (lower error) to bright yellow (higher error) at various $\beta_c = \beta_e$. The error is superimposed to the contour plot of the DiL CET map (black), for easier evaluation of the position of the error maxima. The comparison highlights regions in which the contribution of the time constants is over/underestimated. The results bring new insight into the accuracy of the CET map method.

For heavily stretched transients, the accuracy of the extraction is good; however, already at $\beta = 0.6$, a significant error in the time-constant distribution is introduced. The closer the exponential decay to the ideal case, the higher the error, and the broader the distribution extracted by the approximated methods (see also Fig. 4). In other words, a transient in which both stretched and ideal transients coexist may lead to a significant overestimation of the time-constant distribution. Finally, at $\beta = 1$, the time-constant distribution should correspond to the Dirac Delta function centered in (t_{c0}, t_{e0}).

The method presented in this article is an extension in two dimensions of the method presented in [18] and, as such, can be used for the extraction of the time-constant spectra of more than one trap distribution.

IV. Two-Dimensional Inversion to Study PBI in Power GaN HEMTs

The theoretical insight built in the previous sections helped us understand the physical meaning of the CET map. In addition, the precision of widely used approximation methods has been quantified both in the 1-D and 2-D domains.

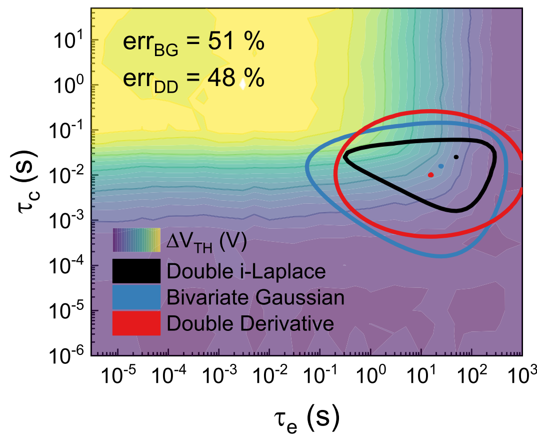

Fig. 7. Contour plot of the extracted time-constant distribution by means of DD (red), BG (blue), and DiL (black) methods.

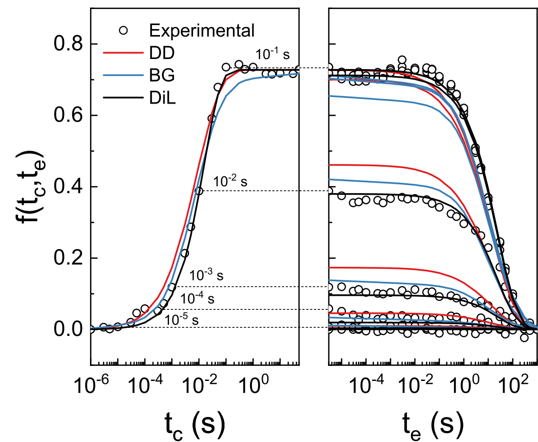

Fig. 8. Comparison between experimentally measured $\Delta V_{TH}(t_c, t_e)$ and reconstructed function.

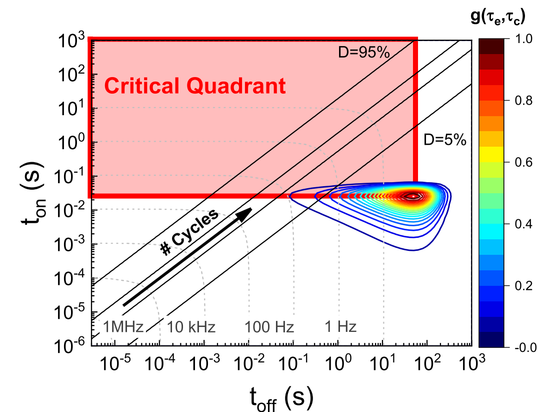

Fig. 9. Cross-comparison between iso-frequencies, iso-duty-cycles, and time-constant distribution in the t_{on}/t_{off} domain.

To conclude our study, the 2-D mathematical framework is used to extract, for the first time, the real CET map from a p-GaN power HEMT subjected to positive bias instability (PBI). The devices under test are similar to the ones presented in [28].

Smaller, faster, and more efficient than their counterpart Si-based components, GaN-based power HEMTs are emerging as excellent candidates for the next generation of power electronics [29], [30], [31], [32], [33].

To date, issues related to threshold voltage instability during BTI (bias temperature instability) are still under study. On the nature of the V_{TH} shift, several publications pointed out the existence of many competing processes taking place when a gate bias is applied [34], [35], [36], [37], [38], [39].

A typical approach to assess the device's dynamic performance is to perform V_{TH} transient measurements. As shown in [40], by repeating the V_{TH} transient measurements with increasing filling times it is possible to obtain a map of the threshold voltage shift $\Delta V_{TH}(t_c, t_e)$.

In our experiment, the device stability is assessed by applying a positive stress bias ($V_G = 3$ V) for different stress times, up to $t_c = 50$ s. The recovery phase is monitored for $t_e = 1000$ s. Similar to the custom-generated function case, the CET map can be built. Once again, the DD, BG, and DiL methods are compared, together with the $\Delta V_{TH}(t_c, t_e)$ experimental map, in Fig. 7. The approximated extraction methods based on DD and BG lead to an absolute error $\approx 50\%$.

A good method to evaluate the accuracy of the map is to reconstruct the $\Delta V_{TH}(t_c, t_e)$ starting from (6). The comparison between simulation and experimental data is shown in Fig. 8. Only the DiL method leads to an excellent fitting.

From Fig. 8, it can be seen that the PBI caused a positive threshold voltage shift in the device under test, whose capture process are orders of magnitude faster than the emission. A physical interpretation of the observed instability can be found in [41].

To conclude our analysis, the experimentally extracted time-constant distribution $g_{DiL}(\tau_c, \tau_e)$ is shown together with the iso-frequency and iso-duty-cycle loci. It should be mentioned that, in real applications, a positive gate bias is applied during the on-phase. Therefore, the higher the duty cycle, the longer the capture time

$$D = \frac{t_{on}}{t_{on} + t_{off}} = \frac{t_c}{t_c + t_e}. \quad (11)$$

The result of the comparison is shown in Fig. 9. The overall behavior of the threshold voltage shift related to PBI at a given duty cycle, depends on the balance between the capture and emission time constants. The peak of the $g_{DiL}(\tau_c, \tau_e)$ corresponds to the region of maximum capture/emission rate.

However, a positive threshold voltage shift will be observed every time the capture processes will not be followed by a sufficiently long emission phase. This condition is highlighted in Fig. 9 with a red square.

As demonstrated in [42], the threshold voltage shift mapped in Fig. 9 can be implemented in a compact model by means of a physically consistent multi-*RC* network. In Fig. 10, a matrix of simulations shows both the effect of the duty cycle and frequency in determining the threshold voltage shift of the device. Remarkably, the cumulative effect resulting from the t_{on}/t_{off} ratio will take place even in the megahertz range. The trajectory of the performance degradation is determined by the duty cycle, while the amplitude of the capture and emission processes per cycle is related to the commutation frequency.

This article has been accepted for inclusion in a future issue of this journal. Content is final as presented, with the exception of pagination.

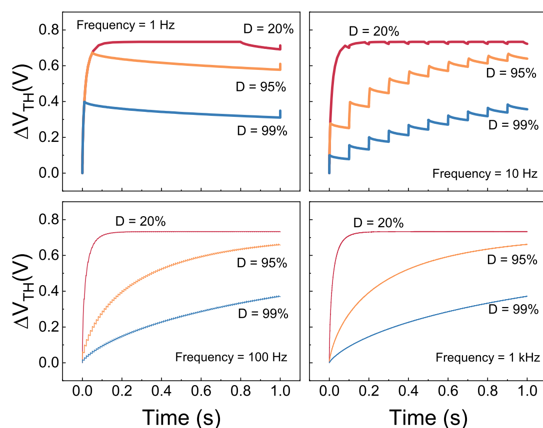

Fig. 10. Matrix of simulations showing both the effect of duty-cycle and frequency in the threshold voltage shift of the device. The frequency defines the amplitude of the trapping/de-trapping kinetics, whereas the duty cycle defines the trajectory of the cumulative shift.

These result highlights how, in circuit design, the choice of frequency and duty cycle draws a trajectory that impacts on the instability of a device, which depends on the balance between trap capture/emission times.

V. Conclusion

Within this article, a novel methodology, for mapping the capture and emission time constants of distributed defects in a wide variety of electronic devices is presented, based on an improved CET map extraction procedure.

Contrary to conventional CET map methods, the proposed approach is based on real-time constant extraction, by means of double inverse Laplace transform. First, to ensure full control of the input parameters, the analysis is carried out on custom-generated functions with different stretching parameters. Then, the developed method is used to extract, for the first time, the full capture/emission time map from a p-GaN power HEMT subjected to PBI.

Finally, we show that a cross-comparison between the iso-frequency, iso-duty-cycle, and the position of the time-constant distribution in the t_{on}/t_{off} domain can give insight into the degradation trajectory of the device at a given working condition.

References

[1] A. Chantre, G. Vincent, and D. Bois, "Deep-level optical spectroscopy in GaAs," *Phys. Rev. B, Condens. Matter*, vol. 23, no. 10, pp. 5335–5359, May 1981, doi: 10.1103/PhysRevB.23.5335.

[2] J. W. Tomm et al., "Deep level spectroscopy of high-power laser diode arrays," *J. Appl. Phys.*, vol. 84, no. 3, pp. 1325–1332, Aug. 1998, doi: 10.1063/1.368201.

[3] T. Mizutani, T. Okino, K. Kawada, Y. Ohno, S. Kishimoto, and K. Maezawa, "Drain current DLTS of AlGaN/GaN HEMTs," *Phys. Status Solidi (A)*, vol. 200, no. 1, pp. 195–198, Nov. 2003, doi: 10.1002/PSSA.200303464.

[4] D. V. Lang, "Deep-level transient spectroscopy: A new method to characterize traps in semiconductors," *J. Appl. Phys.*, vol. 45, no. 7, pp. 3023–3032, Jul. 1974, doi: 10.1063/1.1663719.

[5] G. Meneghesso et al., "Trapping phenomena in AlGaN/GaN HEMTs: A study based on pulsed and transient measurements," *Semicond. Sci. Technol.*, vol. 28, no. 7, Jun. 2013, Art. no. 074021, doi: 10.1088/0268-1242/28/7/074021.

[6] T. Okino, M. Ochiai, Y. Ohno, S. Kishimoto, K. Maezawa, and T. Mizutani, "Drain current DLTS of AlGaN–GaN MIS-HEMTs," *IEEE Electron Device Lett.*, vol. 25, no. 8, pp. 523–525, Aug. 2004, doi: 10.1109/LED.2004.832788.

[7] C. De Santi, M. Buffolo, G. Meneghesso, E. Zanoni, and M. Meneghini, "Dynamic performance characterization techniques in gallium nitride-based electronic devices," *Crystals*, vol. 11, no. 9, p. 1037, Aug. 2021, doi: 10.3390/CRYST11091037.

[8] M. Meneghini et al., "Temperature-dependent dynamic R_{ON} in GaN-based MIS-HEMTs: Role of surface traps and buffer leakage," *IEEE Trans. Electron Devices*, vol. 62, no. 3, pp. 782–787, Mar. 2015, doi: 10.1109/TED.2014.2386391.

[9] S. Mukherjee, E. E. Patrick, and M. E. Law, "Simulation of deep-level trap distributions in AlGaN/GaN HEMTs and its influence on transient analysis of drain current," *ECS J. Solid State Sci. Technol.*, vol. 6, no. 11, pp. 3093–3098, Oct. 2017, doi: 10.1149/2.0211711jss.

[10] A. Y. Polyakov et al., "Current relaxation analysis in AlGaN/GaN high electron mobility transistors," *J. Vac. Sci. Technol. B, Nanotechnol. Microelectron., Mater., Process., Meas., Phenomena*, vol. 35, no. 1, Jan. 2017, Art. no. 011207, doi: 10.1116/1.4973973.

[11] M. Tapajna, R. J. T. Simms, Y. Pei, U. K. Mishra, and M. Kuball, "Integrated optical and electrical analysis: Identifying location and properties of traps in AlGaN/GaN HEMTs during electrical stress," *IEEE Electron Device Lett.*, vol. 31, no. 7, pp. 662–664, Jul. 2010, doi: 10.1109/LED.2010.2047092.

[12] D. Jin and J. A. del Alamo, "Methodology for the study of dynamic ON-resistance in high-voltage GaN field-effect transistors," *IEEE Trans. Electron Devices*, vol. 60, no. 10, pp. 3190–3196, Oct. 2013, doi: 10.1109/TED.2013.2274477.

[13] J. Joh and J. A. del Alamo, "A current-transient methodology for trap analysis for GaN high electron mobility transistors," *IEEE Trans. Electron Devices*, vol. 58, no. 1, pp. 132–140, Jan. 2011, doi: 10.1109/TED.2010.2087339.

[14] D. R. Greenberg and J. A. Del Alamo, "Velocity saturation in the extrinsic device: A fundamental limit in HFET's," *IEEE Trans. Electron Devices*, vol. 41, no. 8, pp. 1334–1339, 1994, doi: 10.1109/16.297726.

[15] C. Chen et al., "The trap locations of GaN HEMT by current transient spectroscopy," in *Proc. ROCS*, 2017, pp. 12–15.

[16] M. Kuzuhara, J. T. Asubar, and H. Tokuda, "AlGaN/GaN high-electron-mobility transistor technology for high-voltage and low-on-resistance operation," *Jpn. J. Appl. Phys.*, vol. 55, no. 7, Jul. 2016, Art. no. 070101, doi: 10.7567/JJAP.55.070101.

[17] D. Bisi et al., "Deep-level characterization in GaN HEMTs—Part I: Advantages and limitations of drain current transient measurements," *IEEE Trans. Electron Devices*, vol. 60, no. 10, pp. 3166–3175, Oct. 2013, doi: 10.1109/TED.2013.2279021.

[18] N. Modolo et al., "Trap-state mapping to model GaN transistors dynamic performance," *Sci. Rep.*, vol. 12, no. 1, pp. 1–10, Feb. 2022, doi: 10.1038/s41598-022-05830-7.

[19] A. B. Bakushinskii, "A numerical method for solving Fredholm integral equations of the 1st kind," *USSR Comput. Math. Math. Phys.*, vol. 5, no. 4, pp. 226–233, 1965, doi: 10.1016/0041-5553(65)90135-7.

[20] D. Yuan and X. Zhang, "An overview of numerical methods for the first kind Fredholm integral equation," *Social Netw. Appl. Sci.*, vol. 1, no. 10, pp. 1–12, Oct. 2019, doi: 10.1007/s42452-019-1228-3.

[21] H. Dubner and J. Abate, "Numerical inversion of Laplace transforms by relating them to the finite Fourier cosine transform," *J. ACM*, vol. 15, no. 1, pp. 115–123, Jan. 1968, doi: 10.1145/321439.321446.

[22] K. Puschkarsky, T. Grasser, T. Aichinger, W. Gustin, and H. Reisinger, "Understanding and modeling transient threshold voltage instabilities in SiC MOSFETs," in *Proc. IEEE Int. Rel. Phys. Symp.*, Mar. 2018, pp. 1–10, doi: 10.1109/IRPS.2018.8353560.

[23] T. Grasser et al., "Analytic modeling of the bias temperature instability using capture/emission time maps," in *IEDM Tech. Dig.*, Dec. 2011, p. 27, doi: 10.1109/IEDM.2011.6131624.

[24] K. Puschkarsky, H. Reisinger, C. Schlunder, W. Gustin, and T. Grasser, "Voltage-dependent activation energy maps for analytic lifetime modeling of NBTI without time extrapolation," *IEEE Trans. Electron Devices*, vol. 65, no. 11, pp. 4764–4771, Nov. 2018, doi: 10.1109/TED.2018.2870170.

[25] T. Grasser, "The capture/emission time map approach to the bias temperature instability," in *Bias Temperature Instability for Devices and Circuits*. New York, NY, USA: Springer, 2014, pp. 447–481.

[26] X. Zheng, S. Feng, Y. Zhang, X. He, and Y. Wang, "A new differential amplitude spectrum for analyzing the trapping effect in GaN HEMTs based on the drain current transient," *IEEE Trans. Electron Devices*, vol. 64, no. 4, pp. 1498–1504, Apr. 2017, doi: 10.1109/TED.2017.2654481.

This article has been accepted for inclusion in a future issue of this journal. Content is final as presented, with the exception of pagination.

[27] X. Zheng, S. Feng, Y. Zhang, and J. Yang, “Identifying the spatial position and properties of traps in GaN HEMTs using current transient spectroscopy,” *Microelectron. Rel.*, vol. 63, pp. 46–51, Aug. 2016, doi: 10.1016/j.microrel.2016.05.001.

[28] N. Modolo et al., “Understanding the effects of off-state and hard-switching stress in gallium nitride-based power transistors,” *Semicond. Sci. Technol.*, vol. 36, no. 1, Nov. 2020, Art. no. 014001, doi: 10.1088/1361-6641/abc456.

[29] Y. Uemoto et al., “Gate injection transistor (GIT)—A normally-off AlGaN/GaN power transistor using conductivity modulation,” *IEEE Trans. Electron Devices*, vol. 54, no. 12, pp. 3393–3399, 2007, doi: 10.1109/TED.2007.908601.

[30] N. E. Posthuma et al., “Impact of Mg out-diffusion and activation on the p-GaN gate HEMT device performance,” in *Proc. 28th Int. Symp. Power Semicond. Devices ICs*, Jul. 2016, pp. 95–98, 2016, doi: 10.1109/ISPSD.2016.7520786.

[31] N. Xu et al., “Gate leakage mechanisms in normally off p-GaN/AlGaN/GaN high electron mobility transistors,” *Appl. Phys. Lett.*, vol. 113, no. 15, Oct. 2018, Art. no. 152104, doi: 10.1063/1.5041343.

[32] A. N. Tallarico et al., “Investigation of the p-GaN gate breakdown in forward-biased GaN-based power HEMTs,” *IEEE Electron Device Lett.*, vol. 38, no. 1, pp. 99–102, Jan. 2017, doi: 10.1109/LED.2016.2631640.

[33] N. Modolo, S. Tang, H. Jiang, C. De Santi, M. Meneghini, and T. Wu, “A novel physics-based approach to analyze and model E-mode p-GaN power HEMTs,” *IEEE Trans. Electron Devices*, vol. 68, no. 4, pp. 1489–1494, Apr. 2021, doi: 10.1109/TED.2020.2992587.

[34] A. N. Tallarico et al., “Gate reliability of p-GaN HEMT with gate metal retraction,” *IEEE Trans. Electron Devices*, vol. 66, no. 11, pp. 4829–4835, Nov. 2019, doi: 10.1109/TED.2019.2938598.

[35] A. Stockman, E. Canato, M. Meneghini, G. Meneghesso, P. Moens, and B. Bakeroot, “Threshold voltage instability mechanisms in p-GaN gate AlGaN/GaN HEMTs,” in *Proc. 31st Int. Symp. Power Semiconductor Devices ICs (ISPSD)*, May 2019, pp. 287–290, doi: 10.1109/ISPSD.2019.8757667.

[36] T. Wu et al., “Forward bias gate breakdown mechanism in enhancement-mode p-GaN gate AlGaN/GaN high-electron mobility transistors,” *IEEE Electron Device Lett.*, vol. 36, no. 10, pp. 1001–1003, Oct. 2015, doi: 10.1109/LED.2015.2465137.

[37] L. Sayadi, G. Iannaccone, S. Sicre, O. Häberlen, and G. Curatola, “Threshold voltage instability in p-GaN gate AlGaN/GaN HFETs,” *IEEE Trans. Electron Devices*, vol. 65, no. 6, pp. 2454–2460, Jun. 2018, doi: 10.1109/TED.2018.2828702.

[38] L. Efthymiou, K. Murukesan, G. Longobardi, F. Udrea, A. Shibib, and K. Terrill, “Understanding the threshold voltage instability during OFF-state stress in p-GaN HEMTs,” *IEEE Electron Device Lett.*, vol. 40, no. 8, pp. 1253–1256, Aug. 2019, doi: 10.1109/LED.2019.2925776.

[39] H. Wang, Y. Liu, F. Ji, H. Li, B. Li, and X. Tang, “Investigation of the threshold voltage instability in normally-off p-GaN/AlGaN/GaN HEMTs by optical analysis,” *Jpn. J. Appl. Phys.*, vol. 60, no. 10, Sep. 2021, Art. no. 104001, doi: 10.35848/1347-4065/AC1DEA.

[40] A. G. Viey et al., “Carbon-related pBTI degradation mechanisms in GaN-on-Si E-mode MOSc-HEMT,” in *IEDM Tech. Dig.*, Dec. 2020, p. 23, doi: 10.1109/IEDM13553.2020.9371938.

[41] N. Modolo et al., “Capture and emission time map to investigate the positive V_{TH} shift in p-GaN power HEMTs,” *Microelectron. Rel.*, vol. 138, Nov. 2022, Art. no. 114708, doi: 10.1016/J.MICROREL.2022.114708.

[42] N. Modolo et al., “Compact modeling of nonideal trapping/detrapping processes in GaN power devices,” *IEEE Trans. Electron Devices*, vol. 69, no. 8, pp. 4432–4437, Aug. 2022, doi: 10.1109/TED.2022.3184622.

Open Access funding provided by ‘Università degli Studi di Padova’ within the CRUI CARE Agreement